UCLA
UCLA Previously Published Works

Title

Hyperbranched Polyglycerol-Induced Porous Silica Nanoparticles as Drug Carriers for Cancer Therapy In Vitro and In Vivo

Permalink

https://escholarship.org/uc/item/97r6592q

Journal

ChemistryOpen, 6(1)

ISSN

2191-1363

Authors

Yang, Yang
Wang, Anhe
Wei, Qiang
et al.

Publication Date

2017-02-01

DOI

10.1002/open.201600072

Peer reviewed

eScholarship.org Powered by the California Digital Library
University of California

ChemPubSoc Europe

DOI: 10.1002/open.201600072

Open Access ChemistryOPEN Full Papers

Hyperbranched Polyglycerol-Induced Porous Silica Nanoparticles as Drug Carriers for Cancer Therapy In Vitro and In Vivo

Yang Yang,[a] Anhe Wang,[a] Qiang Wei,[b] Cathleen Schlesener,[b] Rainer Haag,[b] Qi Li,[c] and Junbai Li*[a, c]

Mesoporous silica-based nanoparticles are generally accepted as a potential platform for drug loading with a lot of advantages, except for their complex purification procedures and structures that are difficult to decompose. In this work, biocompatible hyperbranched polyglycerol is introduced to synthesize mesoporous silica nanoparticles (MSNs). The materials possess good biocompatibility, controlled release, and biodegradability. They also show passive targeting capability through the enhanced permeability and retention effect and can be excreted from the biological system. The method avoids the needs to employ traditional surfactants and complicated purified procedures, which make these MSNs an efficient delivery system for cancer therapy.

1. Introduction

An ideal nanocarrier drug-delivery system for cancer therapy should possess several features, such as 1) enough surface or pore volume to host the required amount of pharmaceuticals, 2) suitable nano-size to realize the enhanced permeability and retention (EPR) effect and to maximize cellular uptake, 3) controllable release in weak acidic environment of tumors, and 4) safe excretion from the biological system.[1] Despite the various methods reported on the preparation of inorganic, organic, or composite nanocarrier drug systems for clinical therapy, it remains challenging to develop a nanocarrier system that possesses all of the features mentioned above. Silica-based porous nanoparticles are popular carriers in drug delivery, as they are generally accepted as biocompatible, porous, and provide a versatile platform for drug loading.[2–8] A silanol-containing surface can be easily functionalized, allowing for a better control over the drug-diffusion kinetics. In the past decade, several synthetic strategies for the fabrication of mesoporous silica nanoparticles (MSNs) have been developed,[9] such as the well-known surfactant-mediated sol-gel method.[10,11] However, surfactants with low biocompatibility are often used during material preparation, and complex synthesis and purification procedures are unavoidable. Otherwise, the MSNs prepared by traditional methods are generally too rigid to decompose over a reasonable period. Although some work has reported that surfactant-mediated MSNs can be degraded in simulated body fluid,[12–14] their degradation takes too long, even more than 1 month. This would limit potential clinical applications of silica-based nanoparticles to some extent.

Recently, some pathways for the synthesis of silica nanoparticles without surfactant involvement have been developed.[15–20] In these methods, sugar, dendrimers, dyes, or other non-surfactant components were employed for the synthesis of silica materials. The synthesized materials are often amorphous, because no micelles or large-scale clusters are formed during the preparation. Therefore, their structures are looser compared with surfactant-mediated MSNs, which would make their decomposition easy in physiological conditions.[16] More importantly, some environmentally friendly molecules can also be used to construct porous silica nanoparticles.[16–18] Therefore, it is unnecessary to remove these assistant molecules, which is different for removing s traditional surfactant template through tough conditions during the preparation of surfactant-mediated MSNs.

Hyperbranched polyglycerol (PG, structural formula shown in Scheme 1a) is a biocompatible, low-cost, and water-soluble macromolecule.[21,22] Our previous work reported that PG can be used as a green template in preparing bulk mesoporous silica in an environmentally benign way.[17] In this work, we synthesized MSNs doped with PG (PGSNs) that were approximately 50 nm in size through an improved method (Scheme 2). The prepared materials possess good biocompatibility, controlled

[a] Dr. Y. Yang, A. Wang, Prof. Dr. J. Li
National Center for Nanoscience and Technology
Zhong Guan Cun, Bei Yi Tiao 11, Beijing 100190 (P. R. China)
E-mail: jbli@iccas.ac.cn

[b] Dr. Q. Wei, C. Schlesener, Prof. Dr. R. Haag
Department of Chemistry and Biochemistry
Freie Universität Berlin, Takustrasse 3, 14195 Berlin (Germany)

[c] Q. Li, Prof. Dr. J. Li
Key Lab of Colloid, Interface and Chemical Thermodynamics
Institute of Chemistry, Chinese Academy of Sciences
Zhong Guan Cun, Bei Yi Jie 2, Beijing 100190 (P. R. China)

Supporting Information for this article can be found under http://dx.doi.org/10.1002/open.201600072.

© 2016 The Authors. Published by Wiley-VCH Verlag GmbH & Co. KGaA. This is an open access article under the terms of the Creative Commons Attribution-NonCommercial-NoDerivs License, which permits use and distribution in any medium, provided the original work is properly cited, the use is non-commercial and no modifications or adaptations are made.

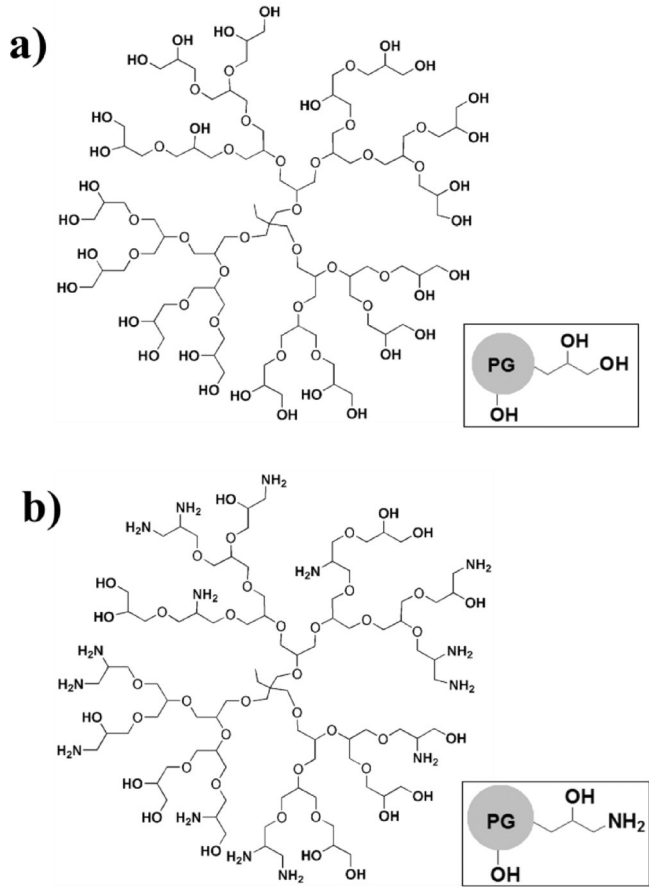

Scheme 1. Representative structure of PG (a) and amino-functionalized PG ($PG–NH_2$) (b); the structures shown represents only one possible isomer or one part of scaffold ($Mw = 10$ kDa).

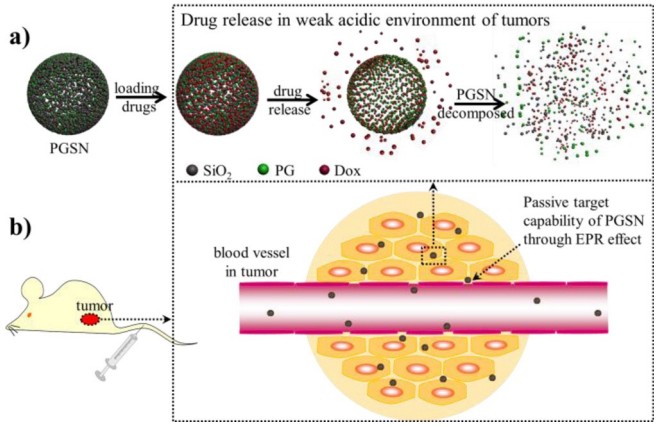

Scheme 2. Schematic illustration of the preparation of PG-doped silica nanoparticles (PGSNs) and their use as drug nanocarriers for tumor treatment.

release, and a desired biodegradation rate. As nanocarriers for cancer therapy, the PGSNs show passive targeting capability through the EPR effect and can be excreted from the biological system. The method avoids any surfactant and complex purified procedures, which make them a multifunctional, biocompatible, and efficient delivery system for cancer therapy.

2. Results and Discussion

Typical silica nanoparticles doped with PG (PGSNs) were synthesized through a one-pot modified sol-gel method. Firstly, amino-functionalized PG ($PG–NH_2$, structural formula shown in Scheme 1 b) was synthesized according to previous work.[23,24] An appropriate amount of $PG–NH_2$ was mixed with silicon precursor (TEOS) overnight under slight vibration. We believe that the nanosilica seeds will be formed immediately, when ammonium hydroxide is added into the mixture of $PG–NH_2$ and TEOS. Then, Si–OH on the surface of the silica seeds interacts with the amino group of $PG–NH_2$ through hydrogen bonding or electrostatic forces. Therefore, amorphous PGSNs were obtained from sol-gel hydrolysis condensation reactions and interactions between silica seeds and $PG–NH_2$ (Scheme 2 a). Typical structures of the PGSNs are shown in Figure 1. They are approximately 50 nm mono-dispersed nanoparticles, which possess mesopores inside them of approximately 2 nm in size. Porosimetry showed that the particles are characterized by a larger surface area (71.88 $m^2 g^{-1}$), in comparison with dense silica particles (16.79 $m^2 g^{-1}$). The size and morphology of silica nanoparticles are different if the amount of added TEOS is increased. As described in the Experimental Section, the diameter increases from 5 to 50 nm if the ratio of $PG–NH_2$/TEOS is changed from 1:0.8 to 1:16 (wt/wt) (Figure S1). It is reported that silica monomers can interact with the amino groups through hydrogen bonds.[25] In this work, we propose that the TEOS molecules will interact with $PG–NH_2$ according to the hydrogen-bonding interaction. Furthermore, $PG–NH_2$ will be doped into the silica nanoparticles after hydrolysis of TEOS. As is known, the PG molecules ($Mw = 10$ kDa used here) are flexible and possess a diameter of approximately 4 nm diameter.[26] Therefore, $PG–NH_2$ will be doped into the silica nanoparticles after the hydrolysis of TEOS, resulting in a loose and porous morphology. The pores of the nanoparticles are likely filled with a lot of PG molecules. Meanwhile, the flexible PG molecules might contain more small molecules for drug-delivery applications.

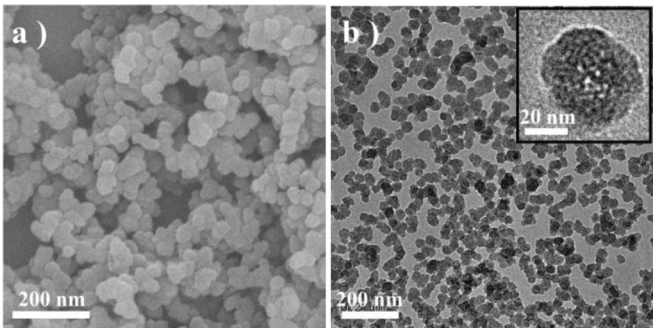

Figure 1. Typical SEM (a) and TEM (b) images of PGSNs-100. The inset image of TEM shows the mesoporous structure of a single particle.

Several control experiments proved that amino-functionalized PG had a decisive role for regulating the PGSN nanostructure. For example, SN-Ctrl-1(silica nanoparticles, control 1) was

© 2017 The Authors. Published by Wiley-VCH Verlag GmbH & Co. KGaA, Weinheim

synthesized by replacing PG–NH_2 with unmodified PG. SN-Ctrl-2 (silica nanoparticles, control 2) was synthesized when there was no PG added. As shown in Figure S2, both SN-Ctrl-1 and SN-Ctrl-2 present solid silica spheres instead of mesoporous silica nanoparticles, which are similar to those of silica spheres synthesized with the Stöber method. It is also shown that the PG component does not work by controlling the structures of silica nanoparticles, because there are no hydrogen bonds formed between PG and the silica monomers.

To verify the components of PGSNs, Fourier transform infrared (FTIR) spectra were measured for PG–NH_2, PGSNs, and calcined PGSNs. In Figure S3, the FTIR spectrum of PG–NH_2 shows characteristic absorbance bands at 2925 and 2875 cm^{-1} (CH_2 stretching). For the spectra of the PGSNs, we can still observe these bands. They are a little weaker than those of pure PG–NH_2 because PG–NH_2 was doped into the silica nanoparticles. These characteristic absorbance bands are not present for the calcined PGSNs when removing the organic component. Further evidence of PG–NH_2 incorporation and information on the inside of the particles was provided by chemical maps obtained by using electron energy loss spectroscopy (EELS). Figure S4 shows a filtered bright-field transmission electron microscopy (TEM) image of PGSNs and the corresponding chemical maps taken from two compositional elements: Si (from silica) and N (from PG–NH_2). From thermogravimetric analysis (TGA) of PGSNs-100, the sample lost about 22% weight from 100 to 600 °C (Figure S5). It does not vary much according to the recipe PGSNs-100 synthesis (18% in theory).

As an ideal drug-delivery vehicle, nanocarriers should be non-toxic and biodegradable. In particular, it is more desirable if they possess a suitable size to enable the EPR effect in cancer therapy.[27–29] It is known that both PG and silica nanoparticles are highly biocompatible materials.[21,22] In addition, based on the size and the structure of the PGSNs, it is promising to use them as drug carriers. Therefore, the properties of PGSNs for controlled release were first investigated. Doxorubicin (Dox), a positively charged anticancer drug, was taken as a model drug to investigate the loading and release behavior from PGSNs. Photographs (the inset image of Figure 2) show that Dox has been loaded into the silica nanostructures with a high efficiency. Interestingly, PGSNs-Dox presents different release behavior at different pH values (the curves in Figure 2). In the case of pH 7.2 buffer, Dox is released slowly from the silica nanostructure. Only 23.8% of the adsorbed Dox is released after 2 weeks. In contrast, in pH 5.0 buffer, 88.6% of adsorbed Dox is released during the same time period. Basically, the PGSNs keep their morphology integrity before and after releasing Dox (Figure S6). Silica nanoparticles have negatively charged surfaces (zeta potential −20.6 mV for calcined PGSNs in water), whereas the charge of the silica nanoparticles becomes neutral at pH 5.0 (zeta potential −1.22 mV for calcined PGSNs in MES buffer), and there is a weak interaction between Dox and silica nanostructures, allowing the Dox to be released more quickly. However, Dox escapes from the silica nanostructures slowly at pH 7.2, owing to the strong static interaction. Also, Dox has a pH-dependent solubility, and this may contribute to the pH dependence of Dox release. This feature of drug release from PGSNs at low pH is very desirable for the acidic cancer microenvironment.

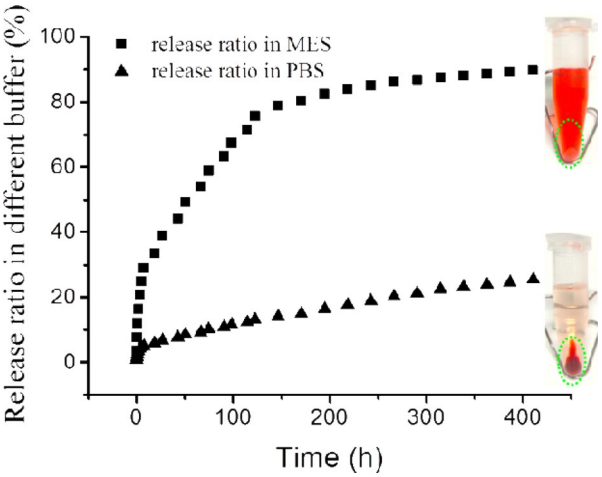

Figure 2. Release profile of encapsulated Dox from PGSN particles in different pH buffers. The inset image shows the supernatant of PGSNs-Dox in the corresponding pH buffer after centrifugation.

Nano-sized and well-dispersed PGSNs are particularly required when they are used as drug carriers to realize the maximization of cellular uptake. Confocal laser scanning microscopy (CLSM) confirms that the PGSNs can carry drugs into the cytoplasm of cancer MCF-7 cells after 3 h co-incubation. As shown in Figure 3, fluorescence signals from Dox-loaded PGSNs (Figure 3c, excitation at 559 nm) were strongly co-localized at the area of treated cells, which suggests efficient interactions between the cells and the particles, whereas the blue fluorescent domains represent the cell nuclei stained by Hoechst 33342 excited by a 405 nm laser (Figure 3a). The green frame represents the cell membranes stained by Alexa 488 excited by a 488 nm laser (Figure 3b). The 3D rebuilding image of the cells also revealed that PGSNs-Dox were endocytosed into the

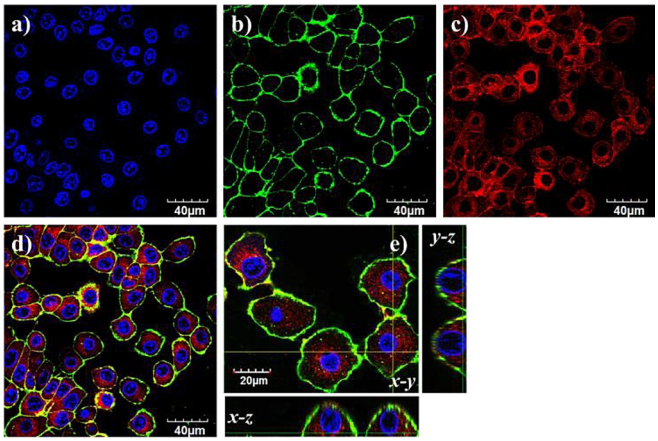

Figure 3. CLSM of MCF-7 cells incubated with PGSN-Dox for 3 h and stained with Hoechst 33342 and Alexa Fluor 488 WGA by exciting at 405, 488, and 559 nm: a) Hoechst 33342-labeled cell nuclei (blue); b) Alexa 488-labeled cell membranes (green); c) PGSN-loaded with Dox; d) the overlapped image; e) enlarged and three-dimensional image. *x*–*y* top view at a given *z* and two other images of the respective *x*–*z* (bottom) and *y*–*z* (right) views along the two yellow lines that represent the position where the stack is cut to form the *x*–*z* and *y*–*z* sections, respectively.

© 2017 The Authors. Published by Wiley-VCH Verlag GmbH & Co. KGaA, Weinheim

cells and located in the cytoplasm (Figure 3e). Another cell line, Hela cells, were also cultured together with PGSNs-Dox. A similar result was obtained (Figure S7). It is noted that most of the Dox would not be released from PGSNs at this beginning stage in cells. However, the drug would be gradually released into the cytosol as time went on. After the PGSNs were labeled with fluorescein isothiocyanate (FITC), the release of Dox from the PGSNs into the cytosol could be observed in real time by using CLSM within 30 h (Figure S8). It proved that Dox was carried into cells with high efficiency by the PGSN carriers. Furthermore, Dox could be released into cytoplasm through the weakly acidic environment of endo-/lysosomes.

To assess the cytotoxicity of PGSNs-Dox and the biocompatibility of the PGSNs in vitro, the viability of MCF-7 cells was analyzed after co-culturing with different concentrations of PGSNs and PGSNs-Dox. As shown in Figure 4 (blue bars), the PGSNs

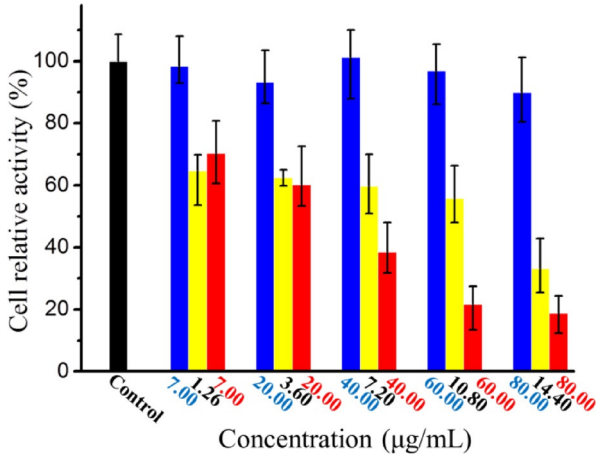

Figure 4. Cytotoxicity of different dosages of PGSNs (blue bar), PGSNs-Dox (0.18 mg Dox per mg of PGSNs, red bar), and Dox (yellow bar, with the same amount of Dox-loaded PGSNs) to MCF-7 cells, the cells treated without PGSNs-Dox or pure Dox as a control.

did not cause any obvious cytotoxicity, as the concentration reaches 0.08 mg mL^{-1}, which indicates that the materials have excellent biocompatibility with the cells. It is reported that silica particles with a smaller size inhibit the growth of cells, to some degree.[30,31] Maybe the PG component reduces the exposure of silanol groups on the silica surfaces, which could decrease the cytotoxicity caused by the silanol groups.[32–34] After drug loading, especially for the high dosage of samples, PGSNs-Dox exhibited a higher cytotoxicity to cells (yellow bars) compared with PGSNs and the same amount of pure Dox (red bars). The cytotoxicity caused by different concentration of PGSNs-Dox and free Dox were analyzed. The *IC*50 value of free Dox is 9.40 μg mL^{-1} (16.21 μM), whereas it is 21.46 μg mL^{-1} for PGSNs-Dox (6.67 μM for the loaded Dox, according to the loading efficiency in PGSNs). It shows that the *IC*50 decreases for loaded Dox in vitro. After being internalized by cells, the PGSNs can protect the fragile drugs and directly release them inside the cells, owing to their pH responsiveness. Furthermore, with the protection of PGSNs, the anticancer drug can also avoid toxicity to normal tissues and organs.

As inorganic drug carriers, silica nanoparticles are generally considered rigid and difficult to degrade. Recently, several groups have reported that silica-based nanoparticles could also be degraded with the help of doped organic components.[14–16,35] However, the degradation rate is so slow, even more than 1 month. In this work, low concentration PGSNs (0.1 mg mL^{-1}) could be degraded, mostly by shaking the culture at 37 °C. As shown in Figure 5, about 80% of the PGSNs

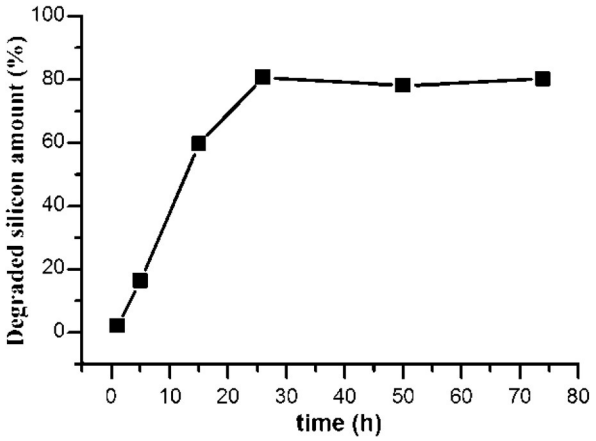

Figure 5. ICP–OES measurement of the amount of degraded silicon of PGSNs in PBS.

were degraded within 30 h. Most PGSN particles were decomposed into scattered fragments (TEMs in Figure S9). It is shown that the PGSNs possess an amorphous and loose nanostructure with the doped PG (Figure S10). In the dilute solution, the PGSNs would be decomposed into fragments or silicate with continuous shaking. It is worth mentioning that the degradation speed of PGSNs is dependent on their concentration in solution. For example, in the drug-delivery experiment mentioned above, PGSNs (1 mg mL^{-1}) are degraded slowly within 2 weeks (Figure S6). It is reasonable that a silicate-saturated solution will be achieved rapidly in highly concentrated PGSN solution, which cannot be decomposed further.

The antitumor activity of PGSNs-Dox in BALB/c mice was evaluated by analyzing the tumor volume in vivo. After treatment with free Dox, PGSNs-Dox, and saline, the average tumor volume of each group at the 11th day of implantation was 588.5, 538.9, and 944.0 mm^3, respectively (Figures 6a and 6b). PGSNs-Dox exhibited a clear inhibitory effect on tumor growth, as compared with the control groups ($p < 0.05$). The tumor inhibition rate is 37.7% for the positive group (treated by Dox) and 42.9% for the experiment group (treated by PGSNs-Dox). Despite the limited improvement, it is still very meaningful for PGSNs used as drug carriers. They can protect the fragile drug, which can cause toxicity to normal organs. As an effective delivery system for anticancer drugs, the carrier should be able to aggregate around the tumor and deliver the drugs into tumor tissues to achieve a tumor-targeted therapy. To assess whether PGSNs could efficiently accumulate in the tumor, the biodistribution of PGSNs was evaluated after injecting a Cy7-labeled PGSN solution into a xenograft mouse model through the tail

© 2017 The Authors. Published by Wiley-VCH Verlag GmbH & Co. KGaA, Weinheim

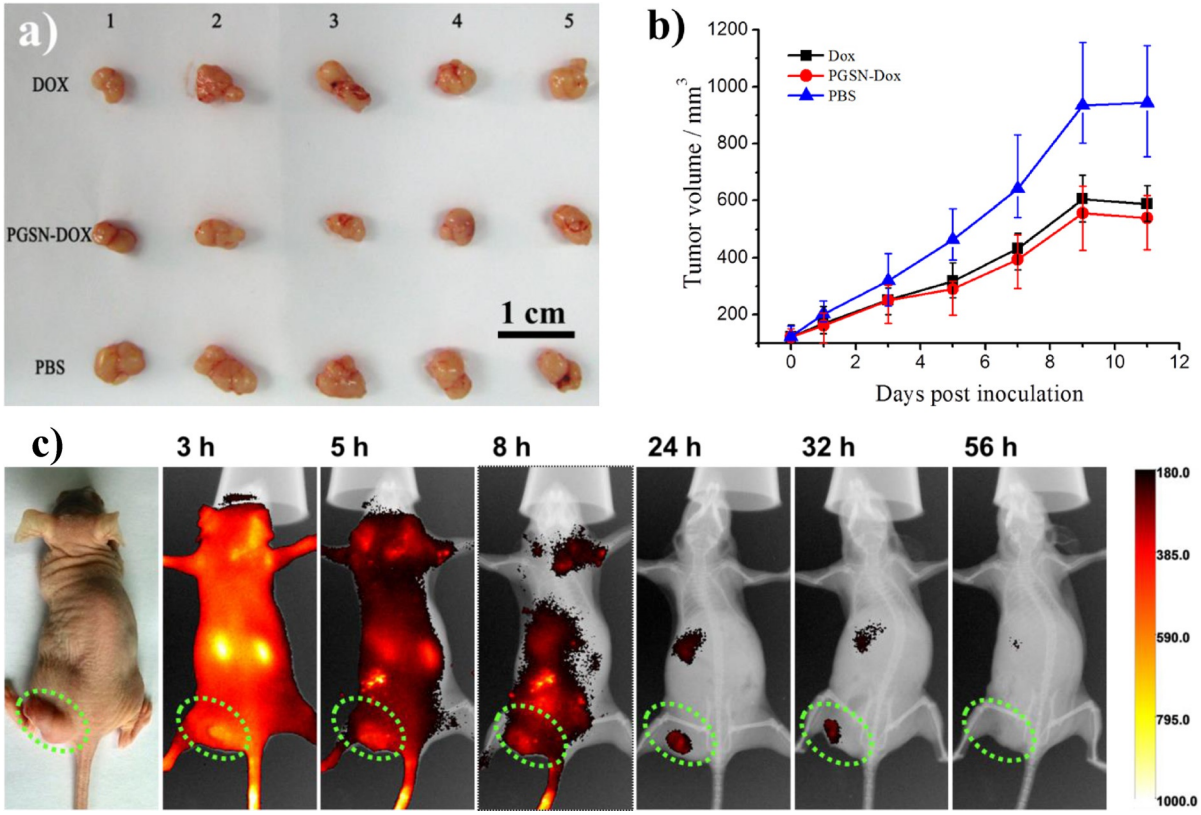

Figure 6. a) Photograph of a tumor isolated from mice after treatment with Dox, PGSNs-Dox and PBS, respectively; b) tumor volume changes over time; c) biodistribution of PGSNs in nude mice, and in vivo real-time images of Cy7-labeled PGSN from approximately 3 to 56 h after intravenous injection. The images are merged from near-infrared fluorescence and X-ray spectra, and the calibration bar was 180–1000 arbitrary units (a.u.).

vein and imaging immediately. As shown in Figure 6c, immediately after intravenous injection, fluorescence emitted from the nanoparticles was easily visualized in the superficial vasculature of the whole body, which might be attributed to the uptake of nanoparticles by the reticuloendothelial system. Subsequently, as blood circulated, the PGSNs were seen to gradually distribute inside kidney, liver, and finally the tumor. Meanwhile, the fluorescence signal was clearly visualized and gradually centralized on the tumor within 32 h, confirming a satisfactory passive targeting capability of PGSNs through the EPR effect. Furthermore, after 56 h, the fluorescence signal of the PGSNs disappeared from the body gradually. During this period, PGSNs were degraded into smaller sizes, which were small enough for renal clearance (< 5.5 nm).[36]

3. Conclusions

We synthesized mesoporous silica nanoparticles doped with functionalized PG (ca. 50 nm in size) through a simple and green synthetic route. The composite nanoparticles present good biocompatibility and biodegradability. Anticancer drugs (e.g. Dox) can be loaded into the nanoparticles with high efficiency and with controlled release in a weak acidic environment. Both experiments in vitro and in vivo proved that this new nanocarrier system can carry the drug into cells or into tumors with passive targeting capability. It has a low toxicity and can be degraded in vivo and excreted from the body through the urinary system. These features make it ideal for therapeutic applications and with great promise for potential cancer treatment.

Experimental Section

Materials

PG (Mw 10 kDa) was synthesized by anionic, ring-opening, multi-branching polymerization of glycidol with slow monomer addition.[37,38] According to our previous work, 10 kDa PG has better dispersity and be synthesized more easily. Tetraethyl orthosilicate (TEOS) was purchased from Acros. Dox and FITC were purchased from Sigma–Aldrich. A cell-counting kit-8 (CCK-8) was obtained from Dojindo Molecular Technologies, Inc. Alexa Fluor 488 WGA and Hoechst 33342 Cell markers were obtained from Molecular Probes Inc. Cy7 NHS ester was synthesized by Okeanos Tech. CO., Ltd. (Beijing, China). Other reagents were obtained from Beijing Chemical Reagent Co. (Beijing, China). The water used throughout the study was purified with a Milli-Q integral A10 system from Millipore Co. (USA).

Preparation of PGSNs

Firstly, we synthesized PG–NH_2 with 30% amine functionality according to the literature.[23,24] For ^{1}H NMR spectra of PG–NH_2, see Figure S11. PG–NH_2 was dissolved into methanol with a concentration of 20 mg mL^{-1} as a stock solution. PGSNs were synthesized by using a modified sol-gel method. Firstly, PG–NH_2 stock solution

© 2017 The Authors. Published by Wiley-VCH Verlag GmbH & Co. KGaA, Weinheim

(600 μL), methanol (2 mL), and a specific volume TEOS were mixed and stirred in a sealed vessel for 12 h. In this recipe, 10, 50, 100, or 200 μL of TEOS was added for parallel controls. Then, a mixture of ammonium hydroxide (1.5 mL) and water (1.5 mL) were quickly added into the above solution and stirred vigorously for 6 h. The products were centrifuged at a high speed (10 000 rpm, 5 min) and washed with methanol and water several times. The purified products were dried in a vacuum oven at room temperature. The final obtained products were marked as PGSNs-10, PGSNs-50, PGSNs-100, and PGSNs-200, respectively, according to the different volumes of TEOS in the recipe.

Guest Molecules Loaded into PGSNs and Released in Response to pH

PGSNs-100 samples (ca. 4 mg) were incubated in 0.5 mg mL^{-1} Dox aqueous solution (1.33 mL) for 24 h. The loading efficiency was calculated according to the change of characteristic absorption of Dox (480 nm) before and after incubation with PGSNs-100. Then, the silica nanostructures were centrifuged and washed with water three times. The samples (denoted as PGSNs-Dox) were split equally into two parts and dispersed into 1.2 mL of either phosphate-buffered saline (PBS) (pH 7.2) or MES buffer (pH 5.0). Therefore, the concentrations of the PGSNs-Dox samples in different buffers were the same (ca. 1.6 mg mL^{-1}). At a preset time point, the sample suspension was centrifuged, and then 0.3 mL of the supernatant was removed. The absorbance at 480 nm of the supernatant was measured using a UV/Vis spectrometer. After that, 0.3 mL of fresh buffer solution was added to the sample suspension. This process was repeated until no further release was observed.

Biodegradability of Silica Nanostructures

The PGSNs-100 sample was dispersed into PBS at a low concentration (0.1 mg mL^{-1}) following shaking of the culture at 37 °C. At a preset time point, a series of aliquots (5 μL) of the solution was removed and dropped on a copper grid for TEM observation. At the same time, 5 mL of the dispersed solution was taken out and filtered by using Millipore tubular ultrafiltration centrifugation modules (molecular weight cut off 10 000). The filtered solution was analyzed for silicon content by using ICP–OES.

Cell Culture

Hela and MCF-7 cells were cultured at 37 °C in a DMEM medium (Gibco BRL, USA) complemented with FBS (10%), L-glutamine (2 mM), penicillin (100 U ml^{-1}), and streptomycin (25 mg mL^{-1}) in a humidified atmosphere with 5% CO_2. For the following experiments, cells were detached from culture flasks by using PBS containing EDTA (0.02%) and trypsin (0.05%), and seeded to a 35 mm glass-bottom Petri dish for CLSM observation or 96-well plates for cytotoxicity measurements. The concentration for seeded cells was 10^5 mL.

Staining of Cells for CLSM Investigation

After the cells were incubated in the logarithmic growth phase, the 2 mg mL^{-1} PGSN-based dispersed sample solutions (50 μL) were added for 4 h of co-culturing. Then, the cells were washed twice with PBS to remove the dispersed nanoparticles and dead cells in the growth media. The cell nuclei and membranes were stained with Hoechst 33342 and Alexa 488 WGA (0.025 mg mL^{-1}, 10 μL) for 15 min, respectively. After that, the cells were washed with PBS three times, and supplemented with fresh cell culture medium. Then, the stained cells were observed by using CLSM.

Cytotoxicity Assay of PGSNs and PGSNs-Dox In Vitro

The cytotoxicity assay was conducted with MCF-7 cells in 96-well plates grown to ~70–80% confluency. Every 4 wells were taken as one group and incubated with different concentration of PGSN, PGSN-Dox and Dox for 48 h, respectively. The Dox loading amount was 0.18 mg per mg of PGSNs. For every well in each group, cells were cultured in 0.007, 0.02, 0.04, 0.06, and 0.08 mg mL^{-1} PGSNs or PGSNs-Dox suspension (in cell culture media) as parallel experiments. At the same time, the same amount of Dox was added to the cells in another group and cultured as a positive control. After 48 h, cells were washed with cell medium. Then, sterile filtered CCK-8 in PBS (10 μL) was added to each well and incubated with the cells for 1 h at 37 °C, followed by measuring the absorbance at 450 nm with ELISA (Tecan infinite 200). Cell viability was expressed as the percentage of viable cells compared with blank control (cells without particles). *IC*50 values were calculated by using IBM SPSS Statistics 22 software.

In Vivo Fluorescence Imaging

Fluorophore Cy7 was labeled on the surface of PGSNs before applying fluorescence imaging in vivo. In detail, the Cy7 NHS ester reacted with PGSNs directly in pH 8.0 buffer solution for 24 h in the dark. Cy7-labeled PGSNs (Cy7-PGSNs) were purified by repeatedly washing with saline before further application. All animal experiments were reviewed and approved by the Animal Care and Use Committee. Tumor-bearing mice were prepared by inoculating 0.2 mL of PBS containing 2×10^6 MCF-7 cells at the left hind leg of female balb/C nude mice (20 ± 2 g), and the tumor was allowed to grow for approximately 7 days. When the tumor volume reached 600 mm^3, 200 μL Cy7-PGSN nanoparticles (in PBS, 1 mg mL^{-1}) was injected through the tail vein. For in vivo imaging, mice were placed on the warmed stage and anaesthetized with 2.5% isoflurane. Image acquisition was performed at different time intervals on an in vivo imaging system. Meanwhile, the fluorescence intensities of the tumor and the background were analyzed by using the corresponding software.

Tumor Therapy In Vivo

When the average tumor volume reached 120 mm^3, the balb/c nude mice ($n=15$) were randomly and equally divided into three groups. The mice in the control group were treated with physiological saline. Free Dox (200 μL, in PBS) or PGSNs-Dox (200 μL, in PBS) was intravenously injected into the tail vein of every animal in the other two respective groups. The concentration of free Dox was 0.12 mg mL^{-1}. The dispersed solution of PGSNs-Dox had a concentration of 2.5 mg mL^{-1}, containing an equal amount of Dox, that is, 0.12 mg mL^{-1}. Mice were treated either with the drug or saline (control) every 2 days with a total of 5 doses per rat. The tumor volume and body weight were measured on alternate days. On the seventh day of post-tumor implantation, the mice were sacrificed randomly, and the tissue was extracted and fixed by 4% formaldehyde solution overnight; tumors were completely excised, and the tumor volume was calculated by using Equation (1):

$$\text{Volume}\ (\text{mm}^3) = V = 0.5 \times a \times b^2 \quad (1)$$

© 2017 The Authors. Published by Wiley-VCH Verlag GmbH & Co. KGaA, Weinheim

where *a* and *b* are the maximum and minimum diameters of the tumor, respectively. The tumor growth inhibition was calculated by using Equation (2):

$$\text{Tumor growth inhibition } (\%) = \left[\frac{(\text{volume in control group} - \text{volume in treated group})}{(\text{volume in control group})}\right] \times 100 \quad (2)$$

where "volume" always refers to the volume of the tumor at the endpoint.

All experiments were performed in triplicate. Statistical significance was evaluated by using the one-way analysis of variance (ANOVA) and Student's *t*-test. Multiple comparisons were statistically analyzed by using SPSS software version 13.0 (significance was established at $P < 0.05$).

Characterization and Instrumentation

UV/Vis spectra were recorded with a Hitachi U-3010 UV/Vis spectrophotometer. CLSM images were taken with an Olympus FV1000 confocal system, which has a 60×oil-immersion objective and a numerical aperture of 1.4. The TEM images and selected-area electron diffraction (SAED) patterns were acquired by using a JEM-1011 and JEM-2011(JEOL, Japan). The scanning electron microscopy (SEM) images were obtained with an S-4800 instrument with 10 kV accelerating voltage (Hitachi, Japan). The degradation of PGSNs was monitored by using both TEM morphology investigation and analysis of the above supernatant through ICP–OES (Thermo Icap 6300). In vivo fluorescence imaging was performed at different time intervals on the in vivo imaging system (FX Pro, Carestream Health). The excitation and emission bandpass filters were at 740 and 760 nm, respectively. The fluorescence intensities of the tumor and the background were analyzed by using corresponding software. Zeta potential and size distribution were documented by using a dynamic light scattering technique (Zetasizer Nano, Malvern).

Acknowledgements

We thank Prof. Yanfei Qi of Jilin University for the experiments in vivo and helpful discussion. This work was financially supported by the National Nature Science Foundation of China (21273055, 21433010, 21320102004 and 21321063), National Basic Research Program of China (2013CB932800), National Key Foundation for Exploring Scientific instrument (2013YQ16055108) and visiting scholar project of the Chinese Academy of Sciences.

Keywords: biodegradation · cancer therapy · drug delivery · hyperbranched polyglycerol · silica nanoparticles

[1] D. Peer, J. M. Karp, S. Hong, O. C. FaroKhzad, R. Margalit, R. Langer, *Nat. Nanotechnol.* **2007**, *2*, 751 – 760.
[2] Z. Li, J. C. Barnes, A. Bosoy, J. F. Stoddart, J. I. Zink, *Chem. Soc. Rev.* **2012**, *41*, 2590 – 2605.
[3] B. G. Trewyn, S. Giri, I. I. Slowing, V. S. Y. Lin, *Chem. Commun.* **2007**, 3236 – 3245.
[4] S. Wang, *Microporous Mesoporous Mater.* **2009**, *117*, 1 – 9.
[5] P. Yang, S. Gai, J. Lin, *Chem. Soc. Rev.* **2012**, *41*, 3679 – 3698.
[6] Y. Yang, J. B. Li, *Adv. Colloid Interface Sci.* **2014**, *207*, 155 – 163.
[7] S. Y. Tan, C. Y. Ang, P. Li, Q. M. Yap, Y. Zhao, *Chem. Eur. J.* **2014**, *20*, 11276 – 11282.
[8] J. Croissant, X. Cattoën, M. W. C. Man, A. Gallud, L. Raehm, P. Trens, M. Maynadier, J.-O. Durand, *Adv. Mater.* **2014**, *26*, 6174 – 6180.
[9] F. Tang, L. Li, D. Chen, *Adv. Mater.* **2012**, *24*, 1504 – 1534.
[10] S. Huh, J. W. Wiench, J.-C. Yoo, M. Pruski, V. S. Y. Lin, *Chem. Mater.* **2003**, *15*, 4247 – 4256.
[11] Q. Cai, Z.-S. Luo, W.-Q. Pang, Y.-W. Fan, X.-H. Chen, F.-Z. Cui, *Chem. Mater.* **2001**, *13*, 258 – 263.
[12] N. Hao, H. Liu, L. Li, D. Chen, L. Li, F. Tang, *J. Nanosci. Nanotechnol.* **2012**, *12*, 6346 – 6354.
[13] Q. He, J. Shi, M. Zhu, Y. Chen, F. Chen, *Microporous Mesoporous Mater.* **2010**, *131*, 314 – 320.
[14] V. Cauda, A. Schlossbauer, T. Bein, *Microporous Mesoporous Mater.* **2010**, *132*, 60 – 71.
[15] J.-H. Park, L. Gu, G. von Maltzahn, E. Ruoslahti, S. N. Bhatia, M. J. Sailor, *Nat. Mater.* **2009**, *8*, 331 – 336.
[16] S. Zhang, Z. Chu, C. Yin, C. Zhang, G. Lin, Q. Li, *J. Am. Chem. Soc.* **2013**, *135*, 5709 – 5716.
[17] Y. Xu, S. Xu, T. Emmler, F. Roelofs, C. Boettcher, R. Haag, G. Buntkowsky, *Chem. Eur. J.* **2008**, *14*, 3311 – 3315.
[18] Y. Wei, D. Jin, T. Ding, W.-H. Shih, X. Liu, S. Z. D. Cheng, Q. Fu, *Adv. Mater.* **1998**, *10*, 313 – 316.
[19] G. Larsen, E. Lotero, M. Marquez, *Chem. Mater.* **2000**, *12*, 1513 – 1515.
[20] A. Mitra, A. Bhaumik, T. Imae, *J. Nanosci. Nanotechnol.* **2004**, *4*, 1052 – 1055.
[21] J. Khandare, M. Calderon, N. M. Dagia, R. Haag, *Chem. Soc. Rev.* **2012**, *41*, 2824 – 2848.
[22] M. Calderón, M. A. Quadir, S. K. Sharma, R. Haag, *Adv. Mater.* **2010**, *22*, 190 – 218.
[23] S. Roller, H. Zhou, R. Haag, *Mol. Diversity* **2005**, *9*, 305 – 316.
[24] J. I. Paez, V. Brunetti, M. C. Strumia, T. Becherer, T. Solomun, J. Miguel, C. F. Hermanns, M. Calderon, R. Haag, *J. Mater. Chem.* **2012**, *22*, 19488 – 19497.
[25] C. Zollfrank, H. Scheel, P. Greil, *Adv. Mater.* **2007**, *19*, 984 – 987.
[26] D. Steinhilber, M. Witting, X. Zhang, M. Staegemann, F. Paulus, W. Friess, S. Küchler, R. Haag, *J. Controlled Release* **2013**, *169*, 289 – 295.
[27] U. Prabhakar, H. Maeda, R. K. Jain, E. M. Sevick-Muraca, W. Zamboni, O. C. Farokhzad, S. T. Barry, A. Gabizon, P. Grodzinski, D. C. Blakey, *Cancer Res.* **2013**, *73*, 2412 – 2417.
[28] H. Maeda, J. Wu, T. Sawa, Y. Matsumura, K. Hori, *J. Controlled Release* **2000**, *65*, 271 – 284.
[29] H. Maeda, T. Sawa, T. Konno, *J. Controlled Release* **2001**, *74*, 47 – 61.
[30] H. Nabeshi, T. Yoshikawa, K. Matsuyama, Y. Nakazato, K. Matsuo, A. Arimori, M. Isobe, S. Tochigi, S. Kondoh, T. Hirai, T. Akase, T. Yamashita, K. Yamashita, T. Yoshida, K. Nagano, Y. Abe, Y. Yoshioka, H. Kamada, T. Imazawa, N. Itoh, S. Nakagawa, T. Mayumi, S.-i. Tsunoda, Y. Tsutsumi, *Biomaterials* **2011**, *32*, 2713 – 2724.
[31] C. Gonzalez, G. Álvarez, D. Camporotondi, M. Foglia, C. Aimé, L. Diaz, T. Coradin, M. Desimone, *Silicon* **2014**, 1 – 6.
[32] Y.-S. Lin, C. L. Haynes, *J. Am. Chem. Soc.* **2010**, *132*, 4834 – 4842.
[33] H. Zhang, D. R. Dunphy, X. Jiang, H. Meng, B. Sun, D. Tarn, M. Xue, X. Wang, S. Lin, Z. Ji, R. Li, F. L. Garcia, J. Yang, M. L. Kirk, T. Xia, J. I. Zink, A. Nel, C. J. Brinker, *J. Am. Chem. Soc.* **2012**, *134*, 15790 – 15804.
[34] Q. He, Z. Zhang, F. Gao, Y. Li, J. Shi, *Small* **2011**, *7*, 271 – 280.
[35] D. Shen, J. Yang, X. Li, L. Zhou, R. Zhang, W. Li, L. Chen, R. Wang, F. Zhang, D. Zhao, *Nano Lett.* **2014**, *14*, 923 – 932.
[36] H. Soo Choi, W. Liu, P. Misra, E. Tanaka, J. P. Zimmer, B. I. Ipe, M. G. Bawendi, J. V. Frangioni, *Nat. Biotechnol.* **2007**, *25*, 1165 – 1170.
[37] A. Sunder, R. Mülhaupt, R. Haag, H. Frey, *Adv. Mater.* **2000**, *12*, 235 – 239.
[38] A. Sunder, R. Hanselmann, H. Frey, R. Mülhaupt, *Macromolecules* **1999**, *32*, 4240 – 4246.

Received: July 5, 2016
Published online on December 12, 2016

 © 2017 The Authors. Published by Wiley-VCH Verlag GmbH & Co. KGaA, Weinheim